Electronic Supplementary Material (ESI) for Physical Chemistry Chemical Physics.

This copy of the ESI replaces the previous version published on 08 April 2022

Supporting Information: Beyond Structural Insight: A Deep Neural Network for the Prediction of Pt $L_{2/3}$-edge X-ray Absorption Spectra

Luke Watson [1], Conor Rankine,[1] and Thomas J. Penfold [1]

List of Figures

[1] Chemistry – School of Natural and Environmental Sciences, Newcastle University, Newcastle upon Tyne, NE1 7RU, UK, tom.penfold@ncl.ac.uk

S1 Supplementary Results

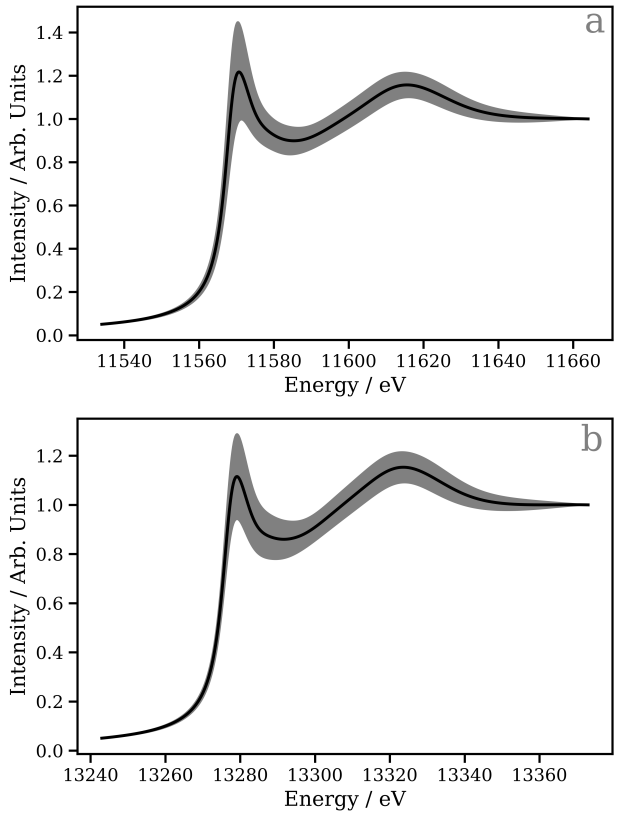

Figure S1: Average (black line) and standard deviation (grey shaded) over all of the Pt a) L_3- and b) L_2-edge XANES spectra contained in the training dataset used in this work.

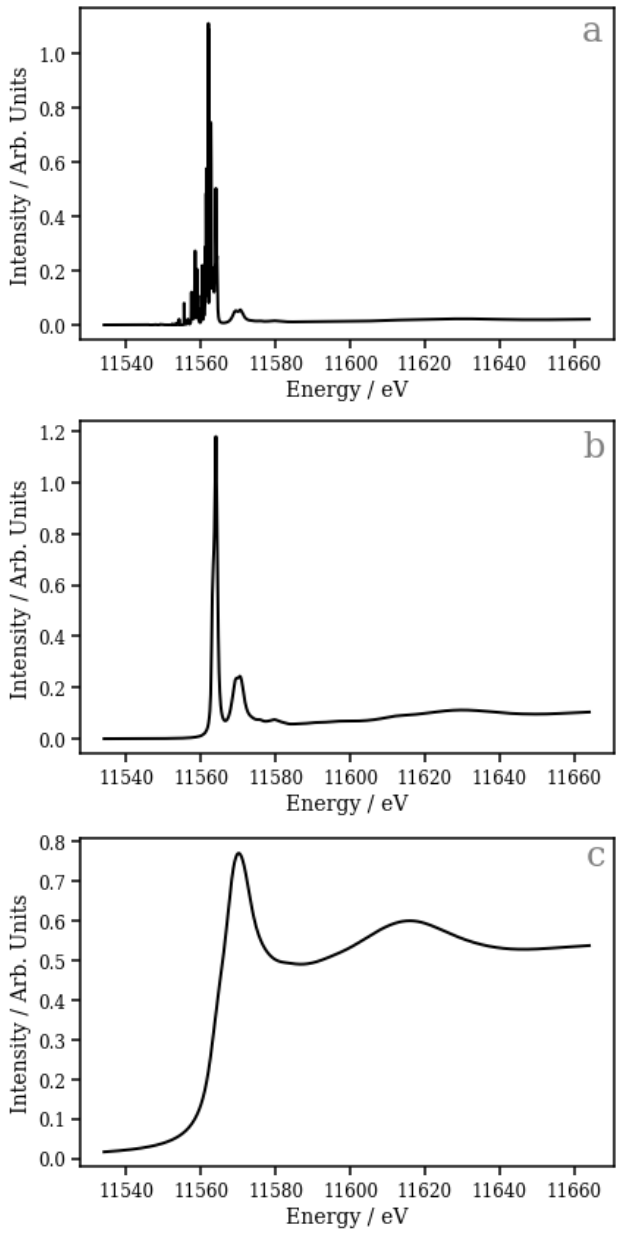

Figure S2: Example absorption cross-sections for the Pt L_2 edge of $C_{38}H_{27}ClO_2P_2Pt$ (CCSD code: BEDMAA) a) without any postprocessing, b) broadened with a fixed-width Lorentzian function (FWHM = 0.5 eV), and c) broadened with an arctangent convolution model.

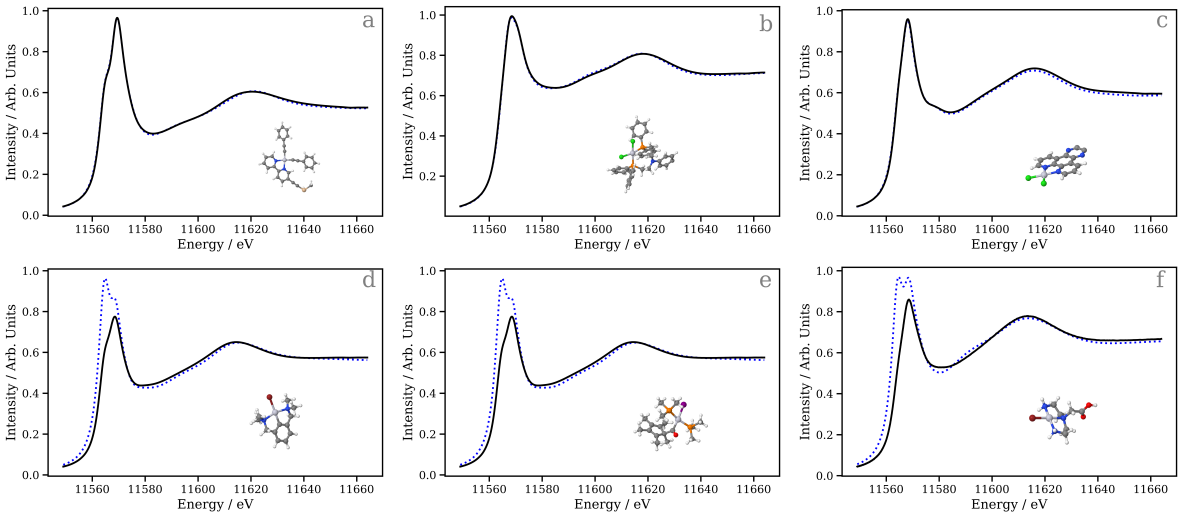

Figure S3: Examples of theoretical target (dashed line) and DNN-predicted (solid line) Pt L_2-edge XANES spectra in a) $C_{31}H_{26}N_2PtSi$ (CCSD code: BAZBIP), b) $C_{34}H_{33}Cl_2NP_2Pt$ (CCSD code: DAFDEW), c) $C_{16}H_8Cl_2N_4O_4Pt$ (CCSD code: IWALEZ), d) $C_{12}H_{19}BrN_2Pt$ (CCSD code: DEGPAG), e) $C_{17}H_{33}IOP_2Pt$ (CCSD code: MIVHAB), and f) $C_6H_{15}BrN_3O_2Pt$ (CCSD code: MUQLOA). The XANES spectra in the upper and lower three panels were drawn from the 1^{st} and 99^{th} centiles, respectively, where DNN estimations are ranked by MSE. In this Figure, the XANESNET model was developed based upon input data which was broadened using the arctangent convolutional model.

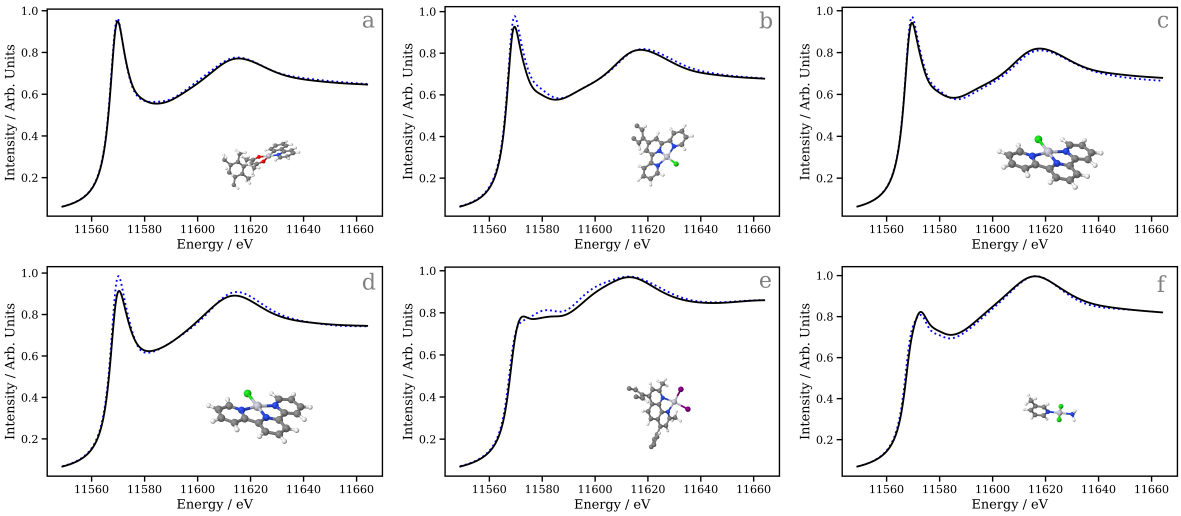

Figure S4: Examples of theoretical target (dashed line) and DNN-predicted (solid line) Pt L_2-edge XANES spectra in a) $C_{44}H_{48}BNO_2Pt$ (CCSD code: DAGCAS), b) $C_{39}H_{36}BClN_3Pt$ (CCSD code: DESQEY), c) $C_{15}H_{11}ClN_3Pt$ (CCSD code: TAXBOM), d) $C_{17}H_{19}F_2N_3OPt$ (CCSD code: TAKWOU), e) $C_{26}H_{20}I_2N_2Pt$ (CCSD code: TAVVOB), and f) $C_6H_{10}Cl_2N_2Pt$ (CCSD code: TECWAA). The XANES spectra in the upper and lower three panels were drawn from the 1^{st} and 99^{th} centiles, respectively, where DNN estimations are ranked by MSE. In this Figure, the XANESNET model was developed based upon input data which was broadened using the fixed-width Lorentzian (FWHM = 0.5 eV) convolutional model. The spectra shown have then subsequently been broadened using the arctangent convolutional model to allow comparison.

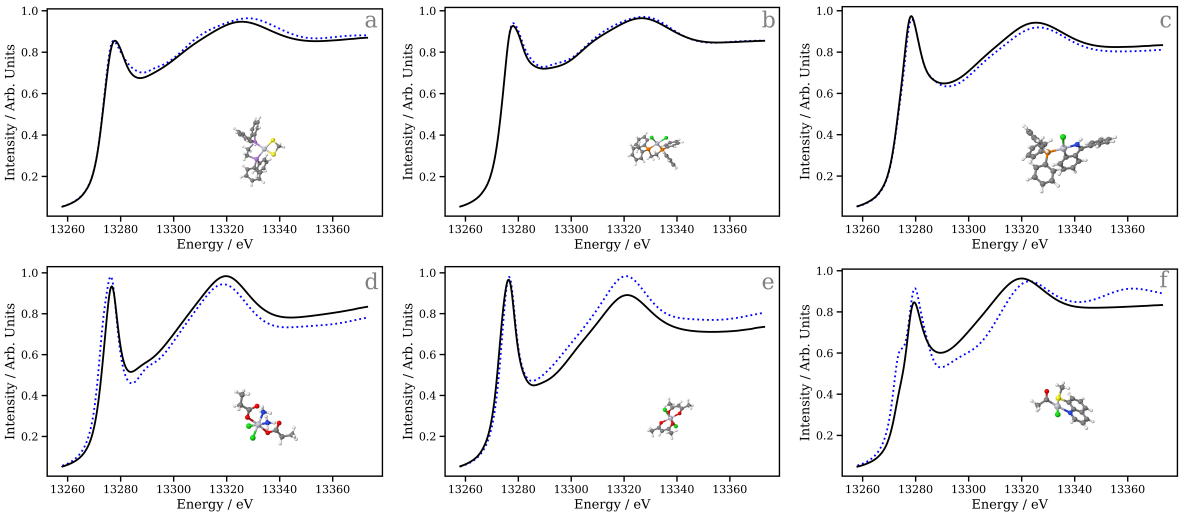

Figure S5: Examples of theoretical target (dashed line) and DNN-predicted (solid line) Pt L_3-edge XANES spectra in a) $C_{27}H_{26}As_2PtS_2$ (CCSD code: CATSOG), b) $C_{26}H_{24}Cl_2P_2Pt$ (CCSD code: DEBXUD), c) $C_{31}H_{25}ClNPPt$ (CCSD code: ZUJPEB), d) $C_6H_{16}Cl_2N_2O_4Pt$ (CCSD code: MIPDOG), e) $C_{10}H_{14}Cl_2O_4Pt$ (CCSD code: NAMLIW), and f) $C_{14}H_{12}F_{14}Pt$ (CCSD code: TATRUC). The XANES spectra in the upper and lower three panels were drawn from the 1st and 99th centiles, respectively, where DNN estimations are ranked by MSE. In this Figure, the XANESNET model was developed based upon input data which was broadened using the arctangent convolutional model.

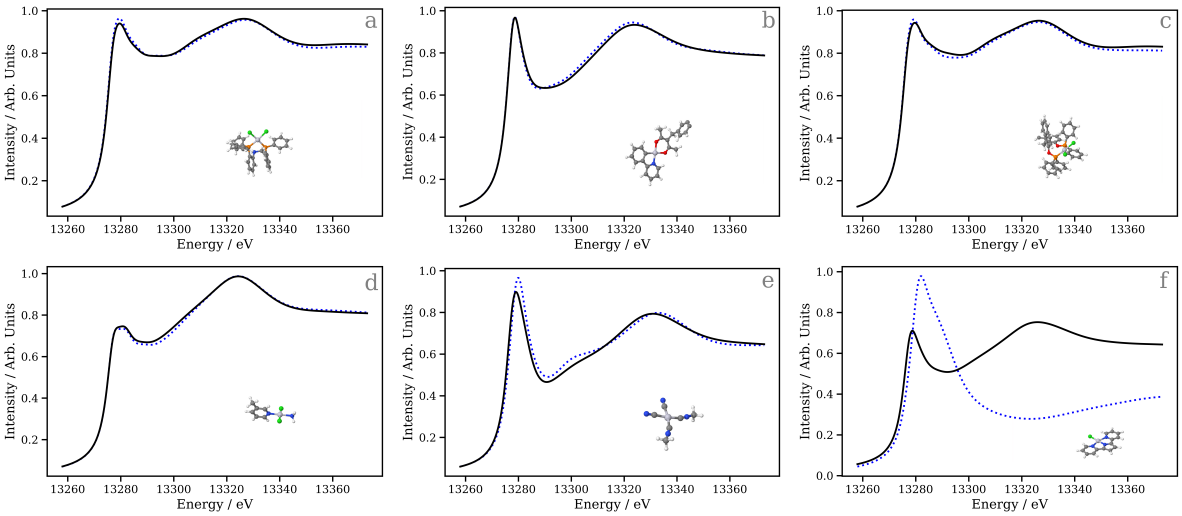

Figure S6: Examples of theoretical target (dashed line) and DNN-predicted (solid line) Pt L_3-edge XANES spectra in a) $C_{31}H_{27}Cl_2NP_2Pt$ (CCSD code: BATNOA), b) $C_{25}H_{23}NO_2Pt$ (CCSD code: MIKFAQ), c) $C_{45}H_{34}Cl_2O_2P_2Pt$ (CCSD code: MUMGEG), d) $C_6H_{10}Cl_2N_2Pt$ (CCSD code: TECWAA), e) $C_6H_6N_4Pt$ (CCSD code: TEFPOK), and f) $C_{14}H_{10}ClN_3Pt$ (CCSD code: TELQEI). The XANES spectra in the upper and lower three panels were drawn from the 1st and 99th centiles, respectively, where DNN estimations are ranked by MSE. In this Figure, the XANESNET model was developed based upon input data which was broadened using the fixed-width Lorentzian (FWHM = 0.5 eV) convolutional model. The spectra shown have then subsequently been broadened using the arctangent convolutional model to allow comparison.

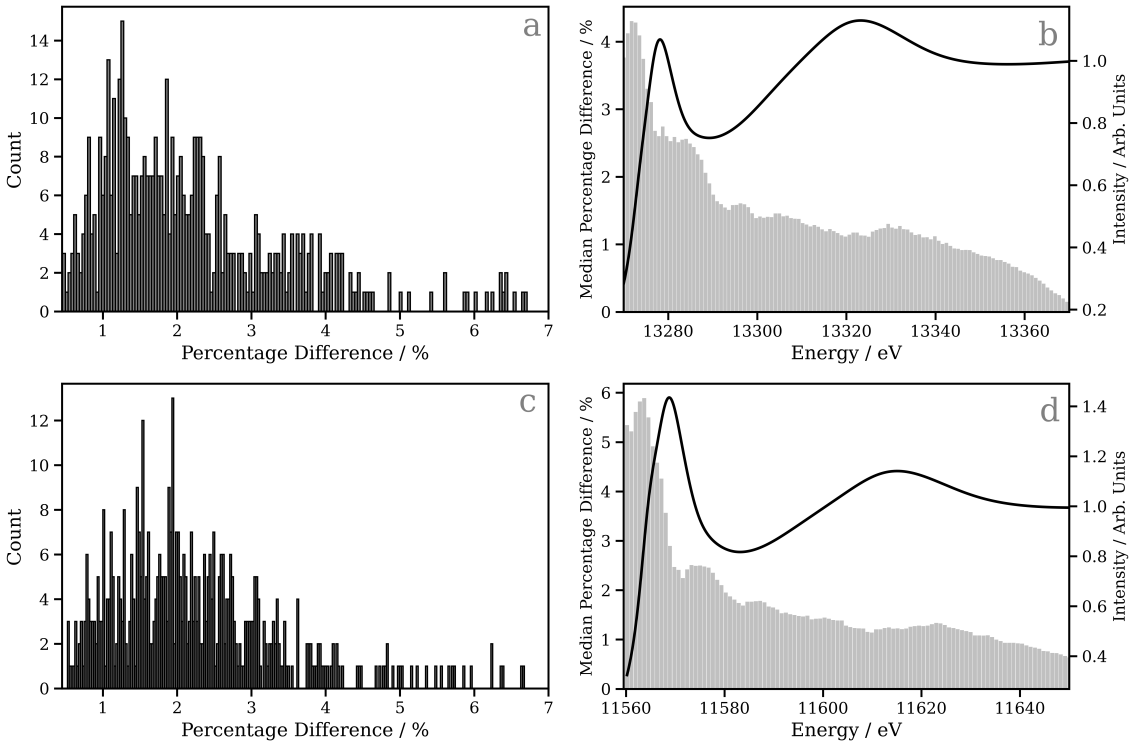

Figure S7: Histogram of the MSEs achieved on 530 held-out DNN-predicted Pt a) L_2- and c) L_3-edge XANES spectra after arctangent convolution; average arctangent-broadened Pt b) L_2- and d) L_3-edge XANES spectrum (solid line) and bar chart of the average MSE point-by-point as a function of energy.

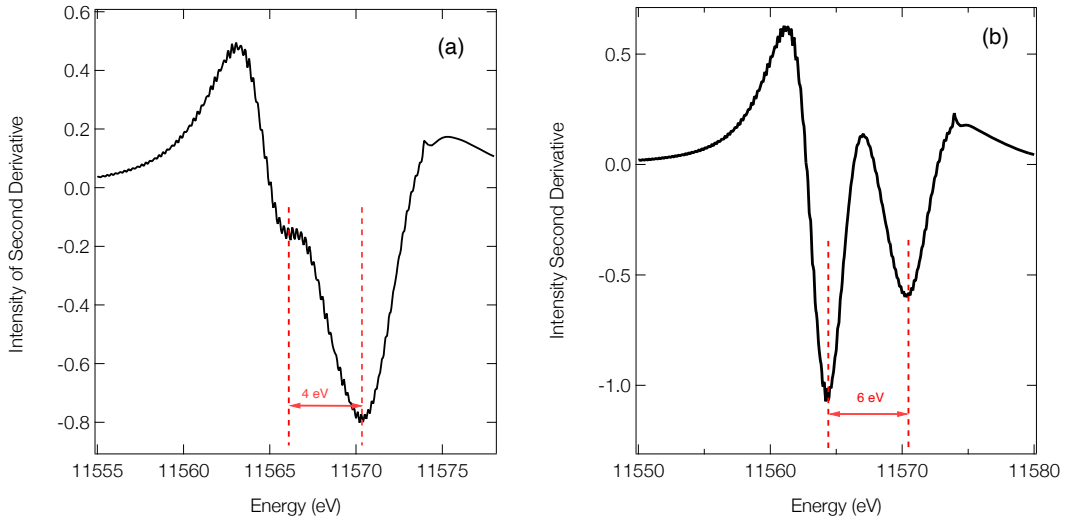

Figure S8: Second derivatives of the normalised DNN-predicted Pt L_3-edge XANES spectra of a) [Pt(PH_3)$_2$(η^2-C_2H_4)] and b) [Pt(PH_3)$_2$(η^2-$C_2(CN)_4$)].

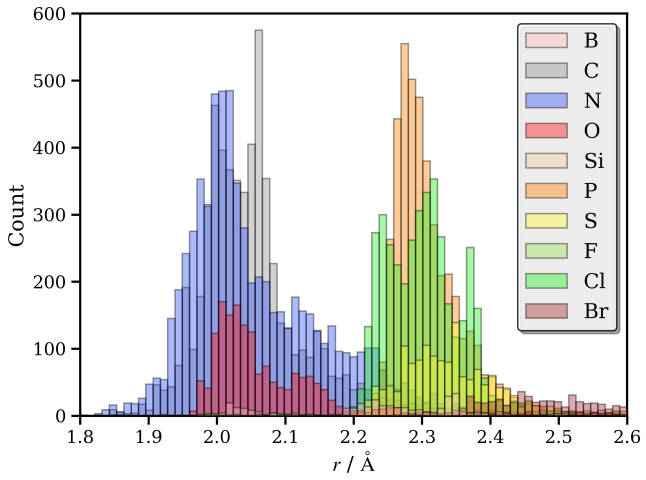

Figure S9: Histogram of atom types and their respective interatomic distances from the Pt X-ray absorption site; data are for the reference (tmQM) dataset.

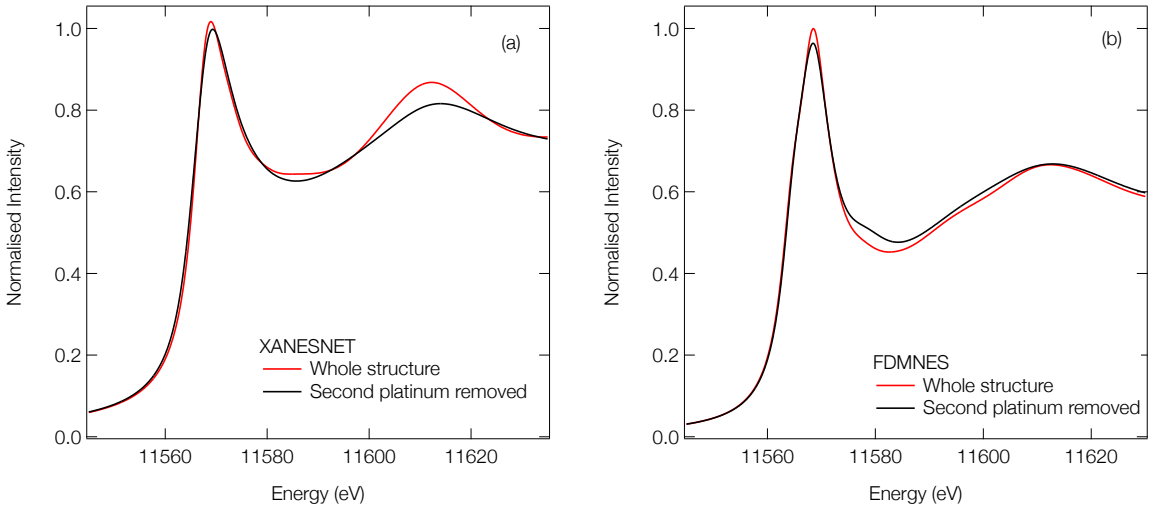

Figure S10: Comparison of the a) DNN-predicted and b) theoretical XANES spectra of [Pt(ppy)(μ-^{t}Bu$_2$pz)]$_2$ with (solid red line) and without (solid black line) the second Pt atom.